Bioactive Materials 6 (2021) 3851–3864

Contents lists available at ScienceDirect

Bioactive Materials

journal homepage: www.sciencedirect.com/journal/bioactive-materials

Covalent functionalization of decellularized tissues accelerates endothelialization

Eleonora Dal Sasso [a,1], Annj Zamuner [b,c,1], Andrea Filippi [c,d,e,f], Filippo Romanato [c,d,f], Tiziana Palmosi [a], Luca Vedovelli [a], Dario Gregori [a], José Luís Gómez Ribelles [g,h], Teresa Russo [i], Antonio Gloria [i], Laura Iop [a,c], Gino Gerosa [a,c], Monica Dettin [b,c,*]

[a] Department of Cardiac, Thoracic and Vascular Sciences and Venetian Institute of Molecular Medicine, Padua, Italy
[b] Department of Industrial Engineering, University of Padua, Padua, Italy
[c] LIFELAB Program, Consorzio per la Ricerca Sanitaria, CORIS, Veneto Region, Italy
[d] Department of Physics and Astronomy "G. Galilei", University of Padua, Padua, Italy
[e] Fondazione Bruno Kessler, Trento, Italy
[f] Institute of Pediatric Research Città della Speranza, Padua, Italy
[g] Center for Biomaterials and Tissue Engineering, CBIT, Universitat Politècnica de València, València, Spain
[h] Biomedical Research Networking Center on Bioengineering, Biomaterials and Nanomedicine (CIBER-BBN), Valencia, Spain
[i] Institute of Polymers, Composites and Biomaterials, National Research Council of Italy, Naples, Italy

ARTICLE INFO

Keywords:
Decellularized pericardium
Decellularized aorta
Covalent functionalization
Endothelialization
REDV
Mechanical analysis

ABSTRACT

In the field of tissue regeneration, the lack of a stable endothelial lining may affect the hemocompatibility of both synthetic and biological replacements. These drawbacks might be prevented by specific biomaterial functionalization to induce selective endothelial cell (EC) adhesion. Decellularized bovine pericardia and porcine aortas were selectively functionalized with a REDV tetrapeptide at 10^{-5} M and 10^{-6} M working concentrations. The scaffold-bound peptide was quantified and REDV potential EC adhesion enhancement was evaluated *in vitro* by static seeding of human umbilical vein ECs. The viable cells and MTS production were statistically higher in functionalized tissues than in control. Scaffold histoarchitecture, geometrical features, and mechanical properties were unaffected by peptide anchoring. The selective immobilization of REDV was effective in accelerating ECs adhesion while promoting proliferation in functionalized decellularized tissues intended for blood-contacting applications.

1. Introduction

The challenge of biomaterial endothelialization affects every year the outcome of thousands of synthetic and biological materials implanted into the cardiovascular system. Due to its specific regulatory activity in thrombotic, fibrinolytic, and inflammatory pathways, the natural healthy endothelium is so far considered the only fully hemocompatible surface. For these reasons, the promotion or restoration of a living endothelium has been widely investigated in those biomaterials intended for blood-contacting applications.

Generally, medical devices as vascular grafts, stents, and glutaraldehyde-treated prosthetic heart valves are scarcely endothelialized and, more often, the process results in partial and unstable lining, which may lead to obstructive thrombi and prosthesis failure. In these conditions, strategies like *in vitro* cell seeding demonstrated to be unsatisfactory in overcoming the poor adhesion proneness of these materials [1–5]. Extracellular matrix (ECM)-derived molecules, such as collagen, laminin, fibronectin, fibrin, heparin, and growth factors [6–10], have been frequently used as coating molecules in order to reproduce the natural subendothelial layer of normal vessels and heart valves. Angiogenic growth factors are currently studied as crucial molecules to promote angiogenesis in bioengineering applications [11,12], whereas gene-eluting stents enriched by DNA encoding for VEGF demonstrated that gene-based strategies may be effective to accelerate

Peer review under responsibility of KeAi Communications Co., Ltd.
* Corresponding author. Department of Industrial Engineering, University of Padua, Via Marzolo, 9 35131, Padova, Italy.
E-mail address: monica.dettin@unipd.it (M. Dettin).
[1] These authors contribute equally to this study.

https://doi.org/10.1016/j.bioactmat.2021.04.003
Received 19 October 2020; Received in revised form 31 March 2021; Accepted 1 April 2021

endothelialization [13]. Specific antibodies were used to target endothelial progenitor cells (EPCs), circulating in peripheral blood, and promote their adhesion to vascular stents [14–17], grafts [18,19], and bioprosthetic heart valves [20,21].

In most of cases, the Achilles' heel of these materials is the lack of bioactive sequences able to coordinate the fine mechanisms of cell adhesion. Therefore, the immobilization of naturally inspired short synthetic peptides, mimicking the adhesive sites of natural proteins, has been introduced in tissue engineering applications.

Several bioactive peptides, including YIGSR, CAG, RGD, and REDV, can be specifically recognized by endothelial cells. The sequence RGD picked out from fibronectin in 1984 as a minimal cell adhesive sequence, is known to be a motif able to bind to several integrin types. Consequently, the RGD tripeptide is by far the most employed adhesive peptide to modify biomaterials [22–24] but RGD can enhance the adhesion of many types of cells and platelets, too; thus, novel peptides should be found to have selective binding for ideally one cell type, in our case endothelial cells, without being involved in clot aggregation and anchoring as RGD sequence is [25,26]. REDV tetrapeptide has been identified for the first time in the type III connecting segment of human plasma fibronectin [27] and has demonstrated to be one of the main sites for the recognition of α4β1 subunits of integrin [28]. This specific interaction leads to the selective adhesion of endothelial cells to fibronectin [29,30]. Owing to its special ability to selectively adsorb and proliferate ECs rather than smooth muscle cells (SMCs), fibroblasts, and platelets [29], REDV has gained much attention in the modification of biomaterials. REDV can capture endothelial colony forming cells (ECFCs) underflow since it can specifically interact with the surface receptor on ECFCs. Furthermore, REDV-grafted hydrogels reduce the ECFC rolling velocity to a significantly greater extent [31].

The efficacy of REDV has been prevalently verified on synthetic materials [29,30,32–35]. This motif incorporated into bioartificial proteins [36] was able to promote HUVEC adhesion. The effort to promote endothelialization of decellularized pulmonary heart valves pre-treated with a solution of REDV peptide did not give significant results compared to a nonfunctionalized group after 1 and 4 h [37]. In the study of Aubin et al. the decellularized tissue was enriched with REDV peptide through physical adsorption. The principal advantage of this strategy is the simplicity of functionalization, but it leads to the random orientation of the bioactive peptide and the reversibility of functionalization. As a consequence, the de-adsorption of the adhesive peptide may inhibit cell adhesion. On the other hand, covalent immobilization is the most irreversible and stable type of immobilization and can control peptide orientation and exposure to cell receptors.

Therefore, this study aims to assess whether and in which conditions the covalent immobilization of EC-selective REDV tetrapeptide on pericardial and aortic valve scaffolds may accelerate the *in vitro* endothelialization. The results of this study demonstrated that the covalent anchoring of REDV to decellularized pericardial and aortic valve scaffolds, carried out in aqueous solution without cross-linkers, accelerates endothelialization. The results also indirectly indicate the importance of the functionalization strategy in the achievement of improved cell-responsive biological scaffolds. A summary of the strategy to convert a biological tissue into a hemocompatible scaffold, as reported in this paper, is shown in Scheme 1.

2. Materials and methods

2.1. Materials

All amino acids used for the peptide synthesis were from Novabiochem (Merck KGaA, Darmstadt, Germany). All other materials were supplied by Sigma-Aldrich (Saint Louis, MO, USA) unless otherwise stated.

2.2. TriCol decellularization

Native bovine pericardia (NBPs) (n = 3) and porcine native aortic roots (NAos) (n = 3) were collected at the local slaughterhouses and transferred to the laboratory in cold phosphate-buffered saline (PBS). Within 1 h from animal death, pericardia and aortic valves were isolated from surrounding fat and connective tissues and shortly rinsed in cold PBS. Homogeneous samples of NBPs were dissected from the left-anterior region of the heart. Both tissues were treated according to TriCol procedure [38–40] (more details are reported in Supplementary Information).

2.3. Evaluation of decellularized scaffold histoarchitecture

Samples (n = 3) were fixed in 4% paraformaldehyde (Panreac AppliChem, Chicago, IL, USA) for 10 min and maintained in 20% sucrose in PBS overnight at 4 °C. Tissues were then snap-frozen in liquid nitrogen fumes after embedding in O.C.T. Compound (Optimal Cutting Temperature Compound, Tissue-Tek, Alphen Aan den Rijn, The Netherlands), and stored at −80 °C. Sections of 5 μm thickness were obtained using a cryostat (Leica Biosystems, Wetzlar, Germany).

Histological analyses were performed using Hematoxylin and Eosin and Alcian Blue staining (Bio-Optica, Milan, Italy). Images were acquired with a light microscope (Olympus BX51, Olympus Corporation, Tokyo, Japan) equipped with a Nikon Eclipse 50i camera and NIS-Elements D 3.2 software (Nikon Corporation Shinagawa, Tokyo, Japan). Indirect immunostaining in tandem with two-photon microscopy (TPM) was adopted to selectively detect basal lamina proteins (laminin, collagen type IV) and fibronectin in combination with second harmonic generation (SGH) and two-photon emitted fluorescence (TPFE), respectively to evaluate collagen type I and elastin pattern [41,42]. As primary antibodies, rabbit polyclonal anti-laminin (1:100, Dako, Agilent Technologies, Santa Clara, CA, USA), rabbit polyclonal anti-collagen IV (1:100, Abcam, Cambridge, UK), and mouse monoclonal anti-fibronectin (1:100, Abcam) were used. Rhodamine (rhod)--conjugated anti-rabbit and anti-mouse were applied as secondary antibodies (1:100 goat anti-rabbit IgG antibody and 1:100 goat anti-mouse IgG antibody, Millipore, Burlington, MA, USA). Primary and secondary antibodies were diluted in 1% (w/v) bovine serum albumin in PBS. Images were acquired at an excitation wavelength of 1200 nm for the SHG signal and 800 nm for TPEF and secondary antibody

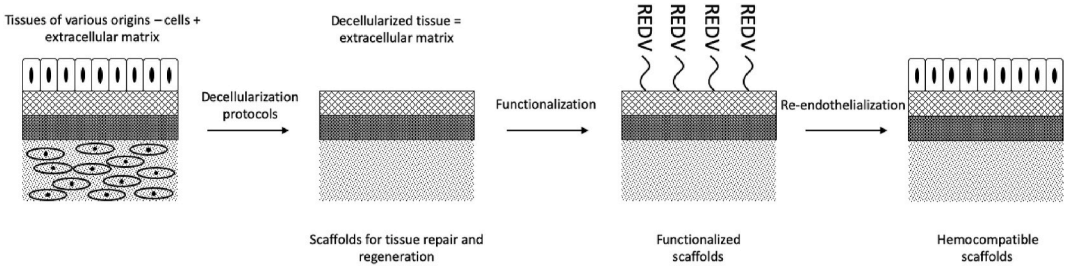

Scheme 1. Development of hemocompatible scaffolds from biological tissues.

fluorophores. A fixed resolution of 1024 × 1024 pixels and an accumulation of 120 frames were selected.

2.4. Peptide synthesis

The tetrapeptide arginine-glutamic acid-aspartic acid-valine (REDV) was synthesized using an automatic synthesizer (Syro I, MultiSynTech GmbH, Witten, Germany) and the solid-phase method via Fmoc chemistry [43]. Two spacers (7-amino heptanoic acid, Novabiochem, Merck Millipore) were introduced between the biologically active sequence and the H-Phe-H resin (NovaSyn® TG, Millipore). Pentamethyl-2, 3-dihydro benzofuran-5-sulfonyl (Pbf) for arginine and *tert*-Butyl (OBut) for aspartic acid and glutamic acid were the side-chain protections used in the current research.

At the end of the synthesis, after Fmoc deprotection, the peptide-resin was divided into two parts. The first part was coupled with 5 (6)-carboxytetramethyl-rhodamine (Novabiochem) (RhodREDV), in order to perform the quantification of the anchored peptide through the quantification of the fluorescence of rhodamine, whereas the second part remained unconjugated. The geometrical, physical, mechanical, and biological properties were evaluated on matrices functionalized with REDV without rhodamine. The biological assays were performed with the REDV without rhodamine because the steric hindrance of the fluorophore might decrease peptide-integrin binding.

Side-chain protections were removed with trifluoroacetic acid (TFA, Biosolve Chimie, Dieuze, France) for 1 h under stirring. The resin was cleaved with a solution of acetic acid, water, methanol and dichloromethane (Biosolve Chimie) (10:5:21:63) for 1 h under stirring.

The purification and characterization of the resulting C-terminal aldehyde peptide are reported in Supplementary Information.

2.5. Functionalization of the biological scaffolds

Purified lyophilized peptides were dissolved in PBS at starting concentration of 10^{-5} M (stock solution). A reducing agent, i.e. sodium cyanoborohydride (Merck Millipore), was added (2.19 mg of $NaBH_3CN$ for 1 mg of peptide). The final solution was then diluted to produce the lower concentration (10^{-6} M). Circular punches of 0.5 cm diameter (Kai Medical Europe, Solingen, Germany) of DBPs and DAos were placed into a 96-well plate (Sarstedt, Nümbrecht, Germany) and functionalized with 100 μl of peptide solution for 24 h at room temperature. The chemical strategy employed is reported in Scheme 2.

After functionalization, the samples were deeply washed in PBS: two times for 30 min at room temperature and one wash overnight at 4 °C, all under constant agitation. Samples were preserved in 3% (v/v) penicillin-streptomycin and 0.25% (v/v) Amphotericin B (Gibco) in PBS at 4 °C until use.

2.6. Quantification of anchored peptide

The yield of functionalization was measured by using RhodREDV. Quantification of RhodREDV peptide covalently linked to functionalized DBPs (n = 3) and DAos (n = 3) was performed using a method already reported [44,45] and was based on TPM-acquired images. The calibration curve was prepared with serial dilutions of free RhodREDV in PBS (from 10^{-5} M to 10^{-10} M). The intensity was measured through Fiji [46]. Six regions of interest (ROIs) were acquired for each dilution of the standard curve, whereas three ROIs were collected for each tested sample. Blank was set with PBS for calibration curve, and the natural fluorescence of pericardial and aortic ECM proteins for differently treated scaffolds. Effective peptide surface densities were calculated multiplying the estimated concentrations by the depth of focal volume (1.5 μm). Based on the results collected, a selective functionalization with a REDV tetrapeptide at 10^{-5} M and 10^{-6} M working concentrations was operated for the decellularized bovine pericardia and porcine aortas.

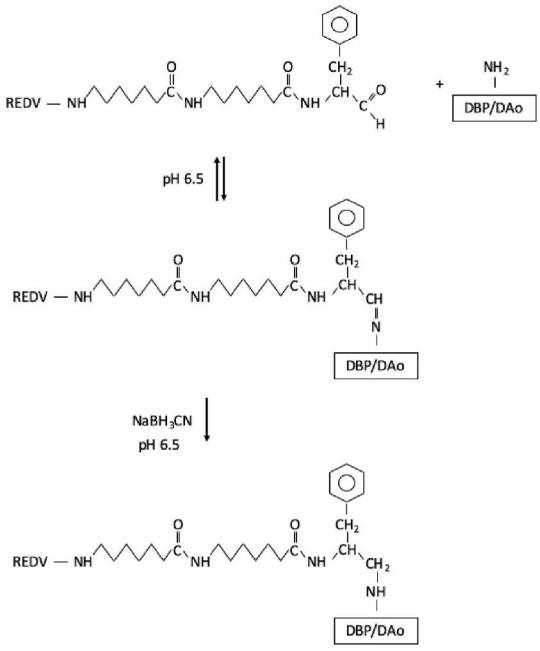

Scheme 2. The chemical strategy of peptide anchoring to the biological scaffolds.

2.7. Geometrical features

Thickness and area of 10^{-5} M, 10^{-6} M REDV-functionalized and control scaffolds (n = 3) were measured to evaluate whether the functionalization could affect the geometrical features of treated tissues. A digital caliper (Mitutoyo, Kawasaki, Japan) was used to assess thickness. Areas were calculated on sample images elaborated in Fiji [46].

2.8. Mechanical compression test

Compression tests were carried out on circular punches of DBPs and DAos at 1 mm/min up to a strain of 0.30 mm/mm. All tests were performed using an INSTRON 5566 testing machine.

The stress (σ) was evaluated as the measured force F divided by the specimen cross-section area (A_0):

$$\sigma = F / A_0 \quad (1)$$

whereas the strain (ε) was calculated as the ratio between the specimen height variation (Δh) and the initial height (h_0):

$$\varepsilon = \Delta h / h_0 \quad (2)$$

2.9. Water contact angle (WCA)

The surface wettability of DBP samples was traced by measuring the static WCA. An OCA20 instrument (Dataphysics), equipped with a CCD camera for the drop shape analysis, was used at 25 °C and 65% relative humidity. Three μL of ultrapure water were applied on different areas of the samples' surface. The static contact angles were then measured on both sides of the two-dimensional projection of the droplet by digital image analysis. Data are reported as the average of at least nine separate measurements on both *serosa* and *fibrosa* sides of DBPs.

2.10. Differential scanning calorimetry (DSC)

The phase transition thermograms of DBP samples were recorded with a DSC 8000 differential scanning calorimeter from PerkinElmer.

Temperature and energy scales were calibrated using the manufacturer's instructions with Indium and Tin as standards. Hydrated samples between 5 and 10 mg of weight were sealed in 30 L aluminum pans. Empty pans were used as references. Thermal analysis was mainly performed to get insight into the denaturation phenomenon of collagen, which is known to occur in the 40–80 °C in the hydrated state and between 180 and 230 °C in the dehydrated state. For this reason, the investigations were performed between 25 and 90 °C with 20 °C/min heating rate.

2.11. Assessment of REDV-functionalization bioactivity and cytotoxicity

EC adhesion was evaluated through viability assays. *In vitro* cytotoxicity tests were carried out according to ISO 10993 requirements [47]. Human umbilical vein ECs (HUVECs) were seeded at a density of 100,000 cells/cm^2 on differently functionalized DBPs (n = 3) and cultivated in static conditions with endothelial growth medium, supplemented with 1% (v/v) penicillin-streptomycin (PromoCell GmbH, Heidelberg, Germany). Polystyrene of tissue culture-treated 24-well plates (Costar®, Corning Incorporated) and cyanoacrylate Super Attack (Loctite, Henkel Italia, Milano, Italy) were used as positive and negative controls, as previously described by Granados et al. [48]. Untreated DBPs were also considered as a further control. Cell viability and adhesion were evaluated using fluorescent Live/Dead staining at 1, 7, and 14 days, according to the manufacturer's protocol (Molecular Probes, Eugene, OR, USA). Samples were analyzed by TPM, acquiring three ROIs for each sample. Due to tissue irregularities or in presence of incline, images were acquired as z-stacks and elaborated as projections with Fiji built-in plugins [46]. Each image was also used to manually calculate the number of live and dead cells by using the cell counter built-in plugin of Fiji. Eventually, the percentage of viable cells was calculated dividing the obtained number of live cells by the total number of cells (i.e., the sum of live and dead cells) as follows: % viable cells = (number of live cells/(number of live cells + number of dead cells)) × 100. The presence of a cell lining was evaluated histologically through hematoxylin eosin staining (BioOptica) on 5 μm fixed cryosections. To evaluate the expression of typical EC markers, like platelet-endothelial cell adhesion molecule (CD31), vWF, and connexin-43 (conx43), a TPM-combined, indirect immunofluorescent analysis was performed by using rabbit polyclonal anti-CD31 (1:50, Abbiotec, San Diego, CA, USA), rabbit polyclonal anti-vWF (1:50, Agilent Technologies) and rabbit polyclonal anti-conx43 (1:100, Abcam) as primary antibodies and rhod-conjugated anti-rabbit (Millipore) as secondary antibodies (1:100), after dilution in 1% (w/v) bovine serum albumin in PBS. Nuclei were counterstained by Hoechst. Images were acquired as described above. Proliferation and cytotoxicity were evaluated with two different colorimetric assays, respectively based on the reduction of 3-(4,5-dimethylthiazol-2-yl)-5-(3-carboxymethoxyphenyl)-2-(4-sulfophenyl)-2H-tetrazolium compound (MTS) and the release of lactate dehydrogenase enzyme (LDH). Both assays are based on the reduction of a tetrazolium salt into formazan, but two different processes are involved: in the first assay, the MTS is reduced by viable cells and, thus, the quantified formazan is directly proportional to their number; in the second assay, the LDH, released by damaged cells, indirectly promotes the enzymatic reduction of the tetrazolium salt by NADH and the resulting formazan amount is proportional to the number of dead cells. Cell media were collected from tested tissues and controls at 24, 48, and 72 h and maintained at −80 °C until further analysis. All tested samples and controls were incubated with MTS reagent following the manufacturer's instructions (CellTiter 96 aqueous solution cell proliferation assay, Promega, Madison, WI, USA) at 1, 3, 7, and 14 days. Absorbance was measured at 490 nm in a plate reader (Bio-Rad, Hercules, CA, USA). Released LDH was quantified with Pierce LDH cytotoxicity assay kit (Thermo Scientific) and the percentage of cytotoxicity was calculated as reported elsewhere [49], after measuring the absorbance at 490 nm with a microplate reader (Bio-Rad).

2.12. Statistical analyses

All data were processed and analyzed with Prism (GraphPad Software). Results are reported as mean ± standard deviation. Data were statistically compared using T-test and analysis of variance (ANOVA). Two-way ANOVA with Bonferroni multiple comparison test was performed to assess the statistical significance of WCA measurements. Results from mechanical compression tests were also analyzed by ANOVA followed by Bonferroni post hoc test. Data from DSC were analyzed by ordinary one-way ANOVA with Tukey's multiple comparison test. A significant level was set at 5%.

3. Results

3.1. Decellularized scaffolds

The histological evaluation confirmed the complete removal of native cells from both pericardial and aortic tissues following the decellularization procedure (Fig. 1, a-h). H&E staining showed the absence of nuclei and the overall tissue architecture appeared well-maintained (Fig. 1, a-d). Alcian blue staining for sulfated and carboxylated mucopolysaccharides and sialomucins exhibited a general discoloration (Fig. 1, e-h). SHG signal appeared unaltered after decellularization: collagen I retained the characteristic wavy pattern in DBP scaffolds and DAo adventitia (Fig. 1, i-u). Similarly, the strong TPEF signal of elastin was maintained particularly for aortic elastic lamellae (Fig. 1, k-l, o-p, s-u). The immunolocalization of laminin (Fig. 1, i-l) and collagen IV (Fig. 1, m-p) demonstrated the preservation of pericardial and arterial basal lamina. A strong positivity for fibronectin can be appreciated in pericardial vessels and *serosa* and in arterial vasa vasorum (Fig. 1, q-u).

3.2. Peptide synthesis

The homogeneity of the REDV fraction used for the functionalization was 99.70%, whereas 89.09% for RhodREDV. The retention time for REDV peptide was 14.94 min (Figure S1). The retention times for RhodREDV peptide were 14.41 min and 16.62 min (Figure S3, two retention times are due to the presence of the two isomers of 5 (6)-carboxytetramethyl-rhodamine in RhodREDV peptide). The experimental masses were 903.73 Da for REDV (theoretical mass: 903.09 Da; Figure S2) and 1316.14 Da for RhodREDV (theoretical mass: 1316.08 Da; Figure S4).

3.3. Quantification of functionalization

RhodREDV bounded on the surfaces of functionalized scaffolds was calculated starting from fluorescent intensity quantifications and reported as the number of peptide moles per cm^2. RhodREDV quantification showed that it was possible to modulate the functionalization yield by varying the initial peptide concentration. Surface densities are reported in Table 1 and Fig. 2.

With respect to the controls (Fig. 2, a, d and g, j), the highest intensity was acquired for 10^{-5} M REDV-functionalized samples for both tissues (Fig. 2, b, e and h, k), whereas with 10^{-6} M working concentration a lower fluorescent signal was observed in treated scaffolds (Fig. 2, c, f and i, l, for DBPs and DAos, respectively).

In the case of DBP scaffolds, only the functionalization with 10^{-5} M concentration allowed to obtain a uniformly distributed fluorescent signal on *serosa* layer (Fig. 2, b-c). On *fibrosa*, the fluorescent pattern was distributed likely following the looser collagen bundles and isolated fibers, as if the peptide had a higher affinity for these structures particularly rich in this layer (Fig. 2, e-f). In the case of DAo scaffolds, the majority of REDV appeared bounded to the intimal surface (Fig. 2, h-i) than adventitia (Fig. 2, k-l), as confirmed by the quantification. The 10^{-5} M RhodREDV functionalization generated the highest values of

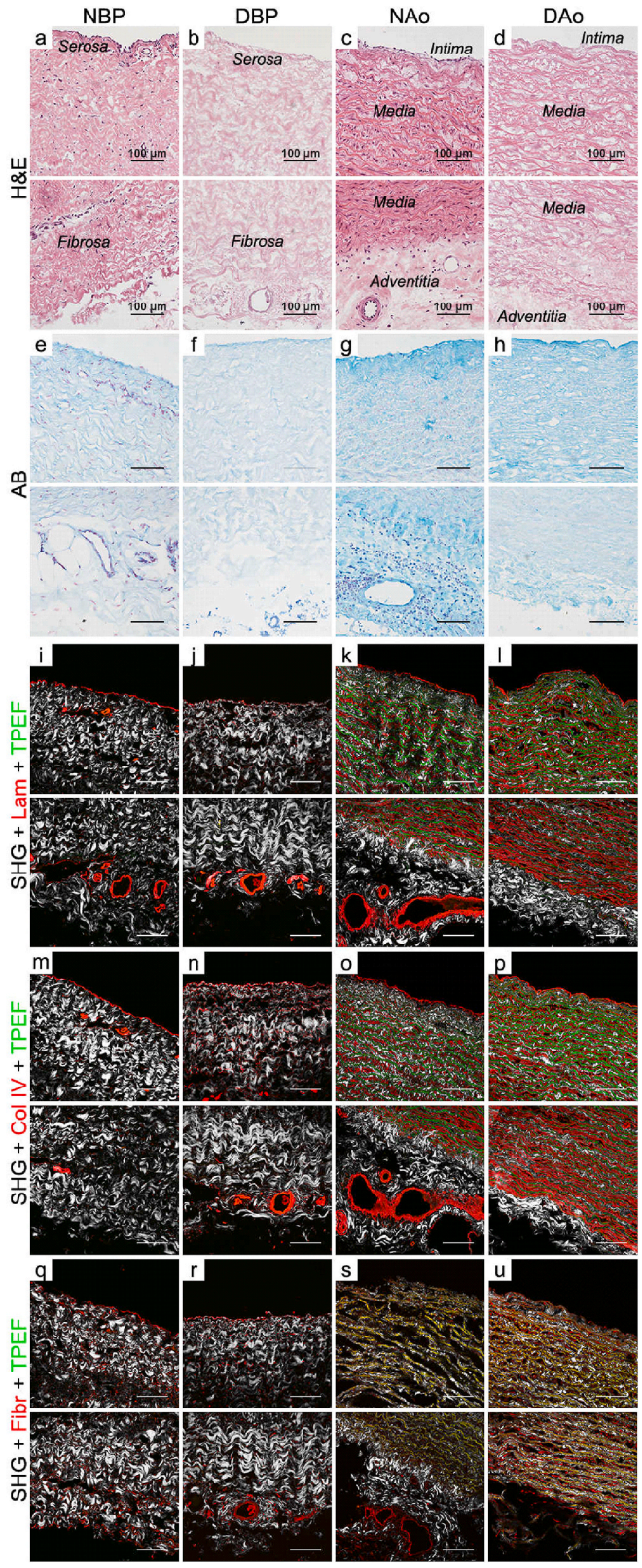

Fig. 1. TriCol decellularization procedure maintained the general tissue histoarchitecture (a–d), whereas seemed to cause a discoloration of alcianophilic components (e–h). Laminin (i–l), collagen IV (m–p) and fibronectin (q–u) appeared maintained.

Table 1
Surface density of REDV on DBPs and DAo scaffolds considering 10^{-5} M and 10^{-6} M as working concentrations.

DBP		
Functionalization concentration [M]	Surface density [mol/cm^2]	
	Serosa	Fibrosa
10^{-5} REDV	$1.17 \pm 0.37 \times 10^{-13}$	$1.01 \pm 0.50 \times 10^{-13}$
10^{-6} REDV	$8.14 \pm 1.77 \times 10^{-16}$	$1.00 \pm 0.62 \times 10^{-15}$
DAo		
Functionalization concentration [M]	**Surface density [mol/cm^2]**	
	Intima	***Adventitia***
10^{-5} REDV	$2.48 \pm 0.30 \times 10^{-13}$	$1.23 \pm 0.38 \times 10^{-14}$
10^{-6} REDV	$3.02 \pm 1.16 \times 10^{-14}$	$2.44 \pm 1.53 \times 10^{-15}$

fluorescence intensity and, therefore, of the amount of bonded peptide to the decellularized scaffolds. Quantified values were statistically different to 10^{-6} M concentration in the case of DBPs and DAo intima.

3.4. Geometrical features and mechanical properties

REDV functionalization did not significantly modify the area (Fig. 3a) and thickness (Fig. 3b) of both DBP and DAo samples in comparison with untreated ones.

J-shaped stress-strain curves were obtained from compression tests on control and functionalized DBPs (Fig. 3, c) and DAos (Fig. 3, d). After an initial upward concavity (toe region), a linear region of the stress-strain curve was evident up to the strain limit of 0.30 mm/mm. The compressive modulus was evaluated as the slope of the linear region of the stress-strain curve. Values of compressive modulus and maximum stress are reported in Tables 2 and 3.

A compressive modulus of 3.68 ± 0.40 MPa and maximum stress of 0.59 ± 0.11 MPa were evaluated for DBP control group (DBP). The functionalization process led to a compressive modulus of 3.57 ± 0.38 MPa (10^{-5} M REDV) and 3.60 ± 0.42 MPa (10^{-6} M REDV), and also to a maximum stress of 0.52 ± 0.09 MPa (10^{-5} M REDV) and 0.54 ± 0.11 MPa (10^{-6} M REDV). However, no statistically significant differences were found among the groups in terms of compressive modulus and maximum stress. With regard to untreated DAo samples (DAo), compression tests provided modulus and maximum stress of 0.80 ± 0.07 MPa and 0.13 ± 0.01 MPa, respectively. Also, in the case of DAo samples, the functionalization process did not significantly affect the values of modulus (0.78 ± 0.07 MPa for 10^{-5} M REDV and 0.81 ± 0.06 MPa for 10^{-6} M REDV) and maximum stress (0.10 ± 0.01 MPa for 10^{-5} M REDV and 0.12 ± 0.01 MPa for 10^{-6} M REDV).

3.5. WCA

Functionalized DBP samples showed significantly different behavior based on the considered side (Fig. 4a): *serosa* appeared more hydrophobic than *fibrosa*. The ordered fibrillar topography of the *serosa* side of the sample, shown in Fig. 2 favors an increase of hydrophobicity as has been shown in different synthetic materials [50–52], the close packing of the fibers, leaving submicron spacing between them, increases air retention and consequently water repulsion at the surface. On the other hand, the disordered arrangement of the fibers in the *fibrosa* side leaves higher inter-fibrillar spaces which do not contribute to hydrophobicity. The same behavior has been shown when comparing ordered and disordered electrospun polylactide mats [50–52].

Increased variability in WCA measurements was observed for the *fibrosa* layer within the same sample, likely depending on the ECM inhomogeneity of this layer.

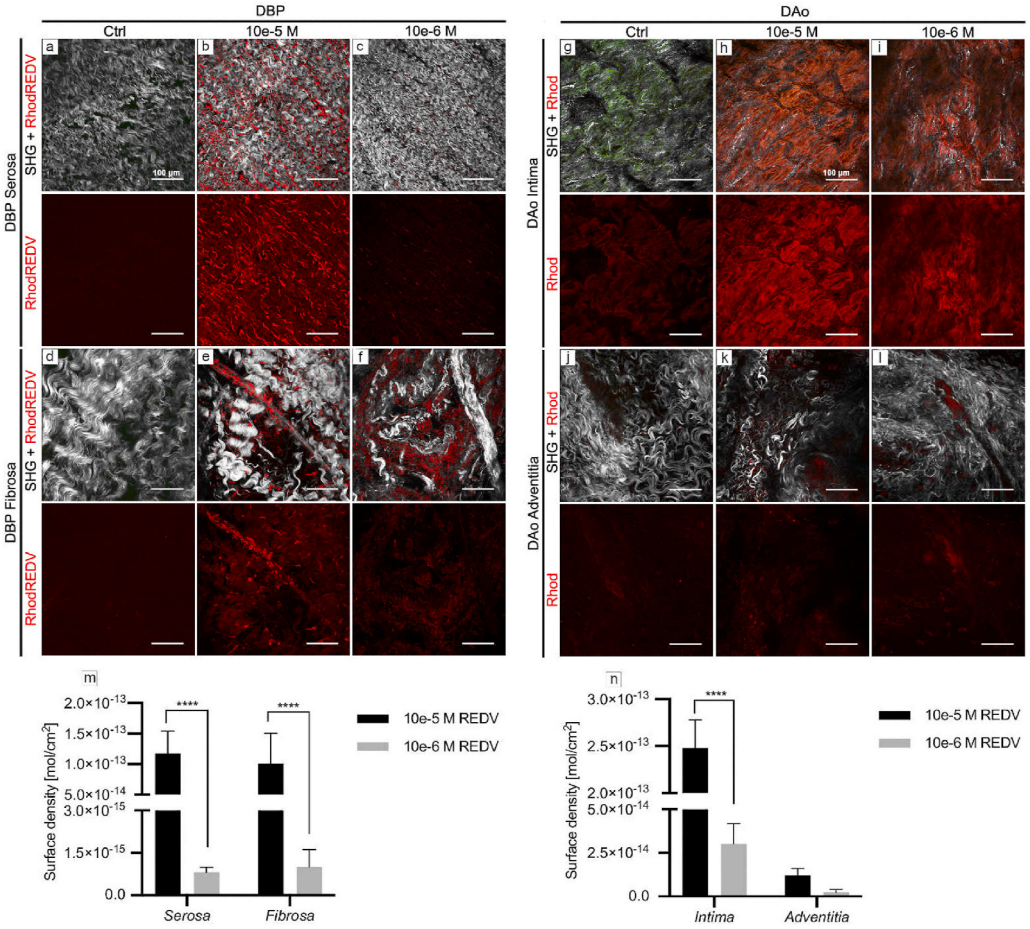

Fig. 2. The concentrations of REDV (10^{-5} M or 10^{-6} M) solution used to treat DBP (a–f) and DAo (g–l) scaffolds have produced different final quantities of peptides bound to the tissues. The surface density of REDV was statistically higher in pericardial tissues functionalized with 10^{-5} M (m–n) in comparison with 10^{-6} M.

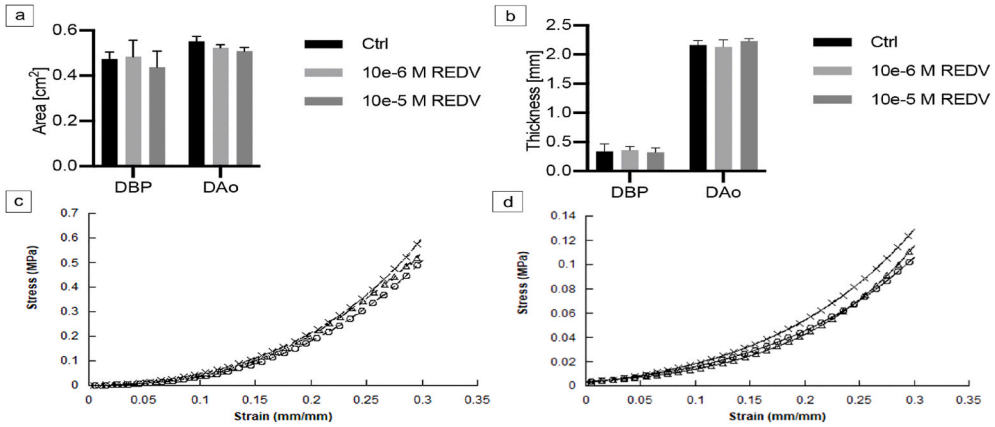

Fig. 3. The functionalization did not affect area (a) and thickness (b) of DBPs and DAos. Considering the compressive mechanical behavior, both functionalized and control DBP and DAo scaffolds showed the typical J-shaped stress-strain curve (c,d): stress-strain curves obtained for DBP control group (x), 10^{-5} M (○) and 10^{-6} M (Δ) REDV functionalized DBPs (c), and for DAo control group (x), 10^{-5} M (○) and 10^{-6} M (Δ) REDV functionalized DAos (d).

REDV functionalization statistically increased the WCA on DBP *serosa* side (p-value < 0.0001), but not for the *fibrosa* layer, whose hydrophilicity seems to be unvaried by the treatment. This feature is also analogous to results found in synthetic fibrillar materials in which the synergy between the combination of topographical and chemical cues to hydrophobicity has been reported [53]. In spite that the functionalization concentration of REDV had a significant influence on the surface density of REDV in the scaffolds, it did not induce significant differences in the measured WCA. One can speculate that in the close-packed fibrils, small amounts of the grafted REDV sequences are sufficient to produce the increase in WCA shown by the experiments.

No direct proportional relationship was documented for the increases of hydrophobicity and peptide surface density on *serosa*.

Table 2
Effect of functionalization on the mechanical properties of DBPs. Results from compression tests performed on control group (DBP), 10^{-5} M and 10^{-6} M REDV functionalized DBPs at 1 mm/min up to a strain of 0.30 mm/mm. Modulus and maximum stress are reported as mean value ± standard deviation. Statistical analysis was performed using ANOVA followed by Bonferroni post-hoc test ($p < 0.05$).

Samples	Compressive Modulus	Maximum Stress
	E (MPa)	σ_{max} (MPa)
DBP	3.68 ± 0.40	0.59 ± 0.11
10^{-5} M REDV	3.57 ± 0.38	0.52 ± 0.09
10^{-6} M REDV	3.60 ± 0.42	0.54 ± 0.11

Table 3
Effect of functionalization on the mechanical properties of DAos. Results from compression tests performed on control group (DAo), 10^{-5} M and 10^{-6} M REDV functionalized DAos at 1 mm/min up to a strain of 0.30 mm/mm. Modulus and maximum stress are reported as mean value ± standard deviation. Statistical analysis was performed using ANOVA followed by Bonferroni post-hoc test ($p < 0.05$).

Samples	Compressive Modulus	Maximum Stress
	E (MPa)	σ_{max} (MPa)
DAo	0.80 ± 0.07	0.13 ± 0.01
10^{-5} M REDV	0.78 ± 0.07	0.10 ± 0.01
10^{-6} M REDV	0.81 ± 0.06	0.12 ± 0.01

3.6. Differential scanning calorimetry

The characterization of DBPs with differential scanning calorimetry showed the presence of an endothermic phenomenon between 60 and 80 °C, which is to be related to collagen denaturation [54,55]. In the literature the denaturation temperature (Td) for hydrated collagen type I is reported at 78.3 °C with an associated enthalpy of 47.8 J/g [56].

The thermograms of all considered samples are reported in Fig. 4b. The endothermic peak related to collagen denaturation is present in all samples of bovine pericardium, but it is interesting to note a slight transition of the denaturation temperature toward higher level for the functionalized samples. The denaturation temperature of collagen in the control (not functionalized DBP) was found at 67.9 °C, as we previously demonstrated [42], with an associated enthalpy of 55.3 J/g, whilst in the case of DBP functionalized with 10^{-6} M and 10^{-5} M REDV solutions, the thermal parameters found were $Td_{10e\text{-}6\ M} = 69.7$ °C with $Hd_{10e\text{-}6\ M} = 41.1$ J/g, and $Td_{10e\text{-}5\ M} = 70.8$ °C with $Hd_{10e\text{-}5\ M} = 43.0$ J/g. The denaturation temperature of functionalized samples was found to be significantly different from the denaturation temperature of the control but not between 10^{-6} M and 10^{-5} M REDV functionalizations.

3.7. Quantification of cell adhesion and cytotoxicity

Results of cell adhesion are reported in Fig. 5. At 24 h and 7 days, 10^{-5} M REDV-functionalized scaffolds showed the highest number of living cells, which progressively decreased in 10^{-6} M REDV-scaffolds, reaching the minimum in the control tissues (Fig. 5, a-h, m-t). In particular, the number of HUVECs was statistically higher for 10^{-5} M REDV-functionalized DBP with respect to the control at 24 h ($p = 0.0259$) and with respect to both control ($p = 0.0182$) and 10^{-6} M REDV-scaffolds ($p = 0.0230$) at 7 days. In case of DAo scaffolds, this trend was significant at 7 days ($p < 0.001$ and $p = 0.0222$, respectively). At 14 days, the number of living cells was not statistically different among the groups for both DBPs and DAos (Fig. 5, i-l and u-x, respectively). Regarding the number of dead cells, for each time-point there were no statistically significant differences among the groups for both tissues (Fig. 5, d, h, l and p, t, x).

Cell viability was generally higher in REDV-functionalized samples and rapidly increased following the first 24 h after the seeding. After 7 days all the values were greater than 95% for all groups and tissues (Table 4).

The progressive endothelialization was confirmed also histologically (Fig. 6a-r). A few rounded cells were visible on samples' surface at 24 h.

A near-continuous lining was present in all groups and tissues from day 7. The quantification of MTS reduction confirmed cell proliferation in functionalized DBP and DAo tissues (Fig. 6 s and t). Functionalized samples generally presented higher proliferation in comparison with unfunctionalized samples and control cells confirming a similar trend to the one observed for cell adhesion. The 10^{-5} M REDV-functionalized DBPs were statistically higher at 7 and 14 days to the controls, whereas 10^{-6} M REDV-functionalized DBPs at 14 days only. Similar results were obtained for DAos, whereas at 24 h both groups of functionalized tissues were statistically higher than unfunctionalized controls. At all endpoints, tissues and positive control presented higher cell proliferation than HUVECs seeded in the negative control conditions. In this case, the complete cell death was visible from day 7 for all groups. The quantification of LDH released in the culture media confirmed negligible cytotoxicity induced by tested biomaterials (Fig. 6, u and v). Functionalized DBP scaffolds presented a trend comparable to their untreated ones: cytotoxicity percentages were negative or positive but close to zero (10^{-6} M REDV-functionalized DBPs at 24 h and 10^{-5} M DBPs at 48 h). The highest values were reached on the first two days, whereas on the third a substantial fall was evidenced. Similar results were obtained for DAo samples. The glue induced 100% of cytotoxicity at all time-points for all tissues. The expression of CD31, vWF, and conx43 in DBPs differently treated is shown in Fig. 7. More in detail, the expression of CD31 and vWF was initially low at 24 h. However, on the following days, these molecules were highly expressed with typical granular aspect on HUVEC cellular membrane. Gap junction protein conx43 confirmed the continuous-like distribution of HUVECs' lining at 7 and 14 days in all groups and tissues.

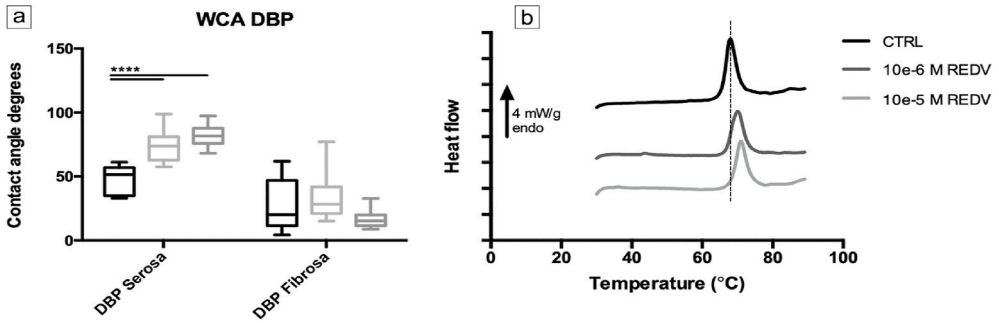

Fig. 4. Water contact angle measurements of functionalized *serosa* and *fibrosa* sides of DBPs (a). Differential Scanning Calorimetry (DSC) thermograms of functionalized DBPs, in the hydrated state recorded at 20 °C/min between 25 °C and 90 °C (b). The legend refers to both graphs (a–b).

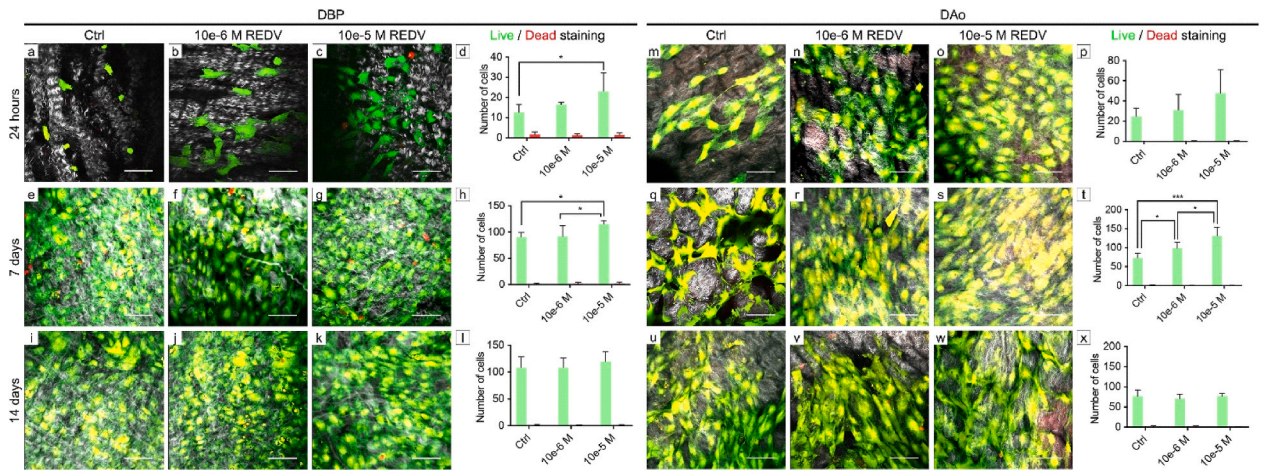

Fig. 5. The number of living HUVECs was statistically higher on 10^{-5} M REDV-functionalized DBPs (a–h) and DAos (m–t) at 24 h and 7 days. At 14 days, there were no significant differences between the groups for both tissues (i-l and u-x). Scale bar = 100 μm.

Table 4
HUVECs' viability at 1, 7, and 14 days following seeding on DBPs and DAo control and REDV-functionalized samples.

DBP			
End point	Ctrl	10^{-6} M REDV	10^{-5} M REDV
24 h	88.3%	93.2%	94.5%
7 days	98.7%	98.1%	98.3%
14 days	99.0%	99.1%	99.3%
DAo			
End point	**Ctrl**	**10^{-6} M REDV**	**10^{-5} M REDV**
24 h	98.7%	87.3%	97.9%
7 days	98.8%	99.3%	99.2%
14 days	98.1%	98.0%	99.7%

4. Discussion

Hemocompatibility is one of the main requirements for the biocompatibility of medical devices intended for blood-contacting applications. The topic has been widely investigated in the fields of medical, engineering, and material sciences but nowadays is still anything but concluded [57–61]. There are many possible gateways to try to solve the quest for blood compatibility, such as act on the coagulation cascade, complement system, and platelets, but none of these strategies demonstrated to be fully effective. Indeed, the principal player is the biomaterial itself. Ideally, in the interaction with blood, it should inhibit and/or prevent the adsorption of proteins triggering the activation of the coagulation and complement systems, hinder platelet adhesion, and support and facilitate the endothelialization process. In the current study, the possibility to accelerate endothelialization by covalent immobilization of EC-selective REDV tetrapeptide was investigated in decellularized pericardial and aortic scaffolds employing HUVECs static cell seeding. In most of the studies, functionalization with adhesive peptides was explored principally on synthetic polymers, because of their lack of bioactive motifs. In these cases, the functionalization required necessarily the chemical modification of the material surface or the inclusion of the peptide into the backbone of polymers. Only a few attempts have been reported for natural scaffolds. The incorporation of PEG into N-(3-dimethyl aminopropyl)-N′-ethyl carbodiimide and N-hydroxysuccinimide (EDC/NHS)-crosslinked collagen sponges was investigated as a platform to enrich this structural protein with bioactive sequences [62]. In a similar approach, decellularized porcine aortic valves were chemically modified with a cyclic RGD [24]. DBP scaffolds were treated with acetic acid and conjugated with RGD motifs using a solution of EDC/NHS [63]. Furthermore, peptide-based functionalization was also evaluated in the case of whole organ engineering. Devalliere et al. [64] demonstrated the feasibility of using the REDV tetrapeptide, fused with an elastin-like peptide, to improve the re-endothelialization of the vascular tree in an acellular rat liver through endothelial perfusion. Our experience is based on a different approach. In our case, the synthesized REDV was immobilized on DBPs by taking advantage of the aldehyde group, at the peptide C-terminal, and the primary amine (ε-amino groups) of lysine and hydroxylysine abundant in the scaffolds as residues of collagen molecules [65]. Besides the use of a reducing agent to obtain an irreversible covalent bond, the functionalization did not require any chemical able to crosslink or denature the DBP. Furthermore, the possibility of cross-reactions between two REDV molecules, due to the Arg side-chain presence in the sequence, is remote mainly due to the high pKa value of the guanidinium group (12.5) but also to the dilute peptide solution (10^{-6} or 10^{-5} M) that discourages the dimerization. The anchoring strategy choice is justified by the effort to preserve the promising biological characteristics and the structural integrity of biological scaffolds. The physical and biological properties of TRICOL DAo and DBP have been widely investigated in recent studies by Iop et al. [39] and Zouhair and colleagues [40]. The results showed intact ECM composition and structure, biomechanical properties, and appealing bioactive properties, thus confirming the suitability of these tissue scaffolds in reconstruction and replacement applications. Decellularized scaffolds offer an adequate milieu for endothelial cell adhesion and survival, as observed in these *in vitro* and *in vivo* studies [39,40,64]. Indeed, REDV biofunctionalization proved to accelerate the endothelialization process, which is of paramount relevance for clinical translation. In this work, TPM analyses performed to evaluate the integrity of collagen I, elastin, and basal lamina elements confirmed the maintenance of these ECM main constituents. Moreover, sample thickness and area were not affected by REDV functionalization. Although morphological analyzes indicated that the scaffold's structure was not altered by functionalization, significant differences in REDV-functionalized pericardium were found in terms of collagen denaturation temperature that appeared to be higher when compared to unfunctionalized DBP suggesting a stabilization of the functionalized collagen compared to the control.

The quantification of the linked peptide was performed with an innovative method based on the use of TPM and the acquisition of the TPEF by the rhodamine-labeled REDV. The development of a new technique was necessary to effectively distinguish the contribution of the peptide from the endogenous matrix one. The evaluation of the FTIR spectra, often adopted in other studies for this purpose [23,24,66,67], was not feasible due to the similarity between the target molecule and the biological matrix. The fluorescence of conjugated peptides was

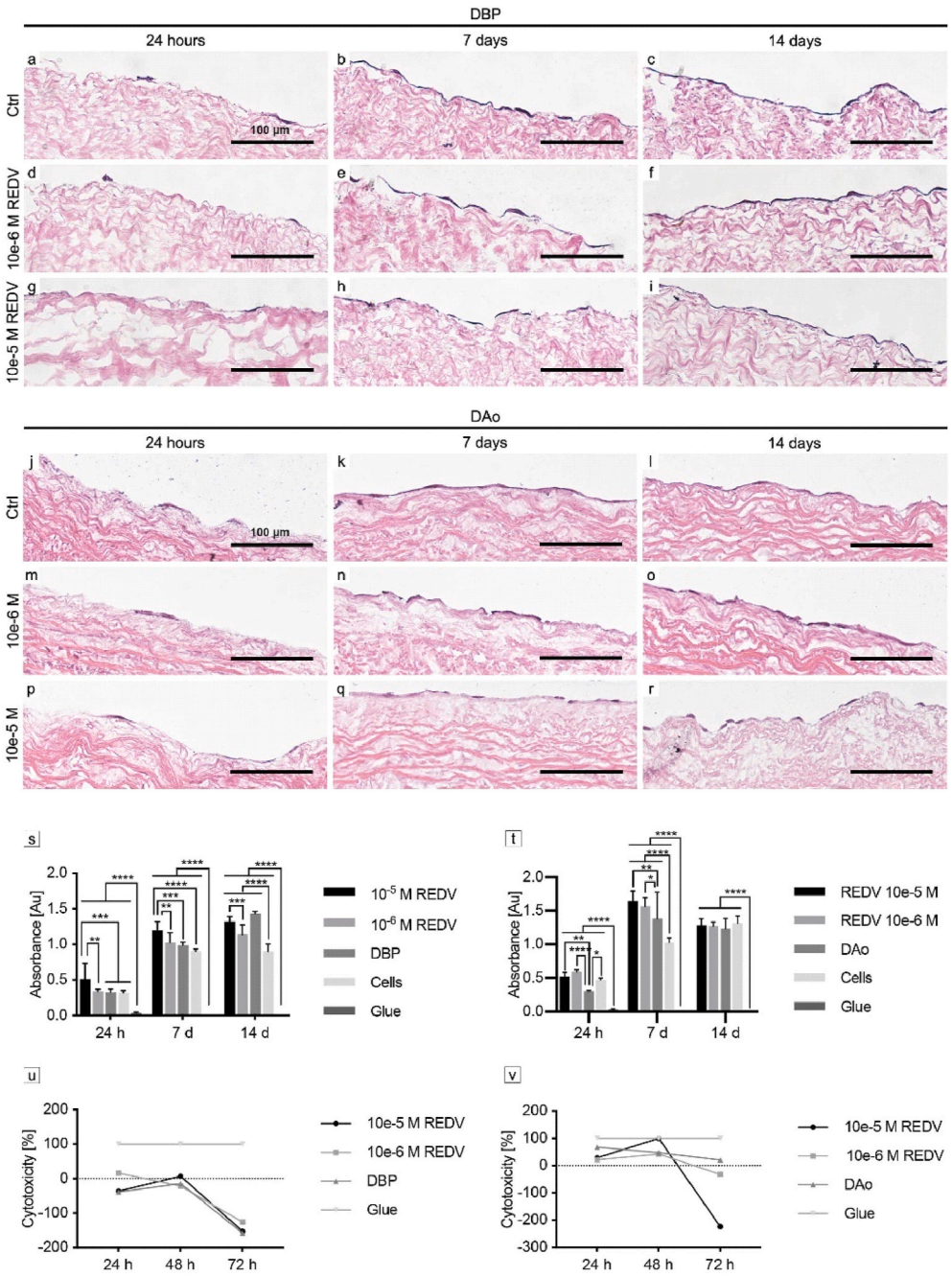

Fig. 6. HUVECs formed a continuous-like cell lining after 7 days, in all groups and tissues (a–r). Cell proliferation was generally higher in 10^{-5} M REDV-functionalized tissues (s, t), and cytotoxicity levels decreased over the considered time-points (u, v).

evaluated in the literature in several works [32,63,68,69]. However, an effective quantification, based on a calibration curve, was performed only in one case [70]. Our results confirmed that, independently from the concentration of peptide used for the functionalization (10^{-5} and 10^{-6} M REDV, in our case), the final amount of peptide anchored into the matrix is inferior to the initial one. The highest functionalization of both sides of the pericardium was achieved with the highest peptide concentration. Furthermore, the localization of RhodREDV by TPM allowed appreciating its distribution on the collagen bundles, thus confirming the efficacy of the chemical approach utilized for biofunctionalization.

On the other hand, over the past years, different kinds of experimental tests have been performed to assess the preservation of the mechanical properties of the investigated tissues, also focusing on several technical considerations.

After the decellularization process, the possibility to maintain the mechanical properties of the native tissue plays a key role in ensuring an appropriate functionality [71,72].

In particular, it is well known how a fundamental part of the decellularization assessment consists in the analysis of the alteration of the decellularized ECM in terms of composition, structure, and mechanical features.

In general, the evaluation of tensile strength, elastic and viscous moduli, stiffness or yield strength is of great interest, as these properties are regulated by the main ECM structural proteins. This clearly stresses the important role of the structure-mechanics relationship [71,72].

The tensile strength of natural and chemically modified bovine pericardium was already analyzed through non-destructive and

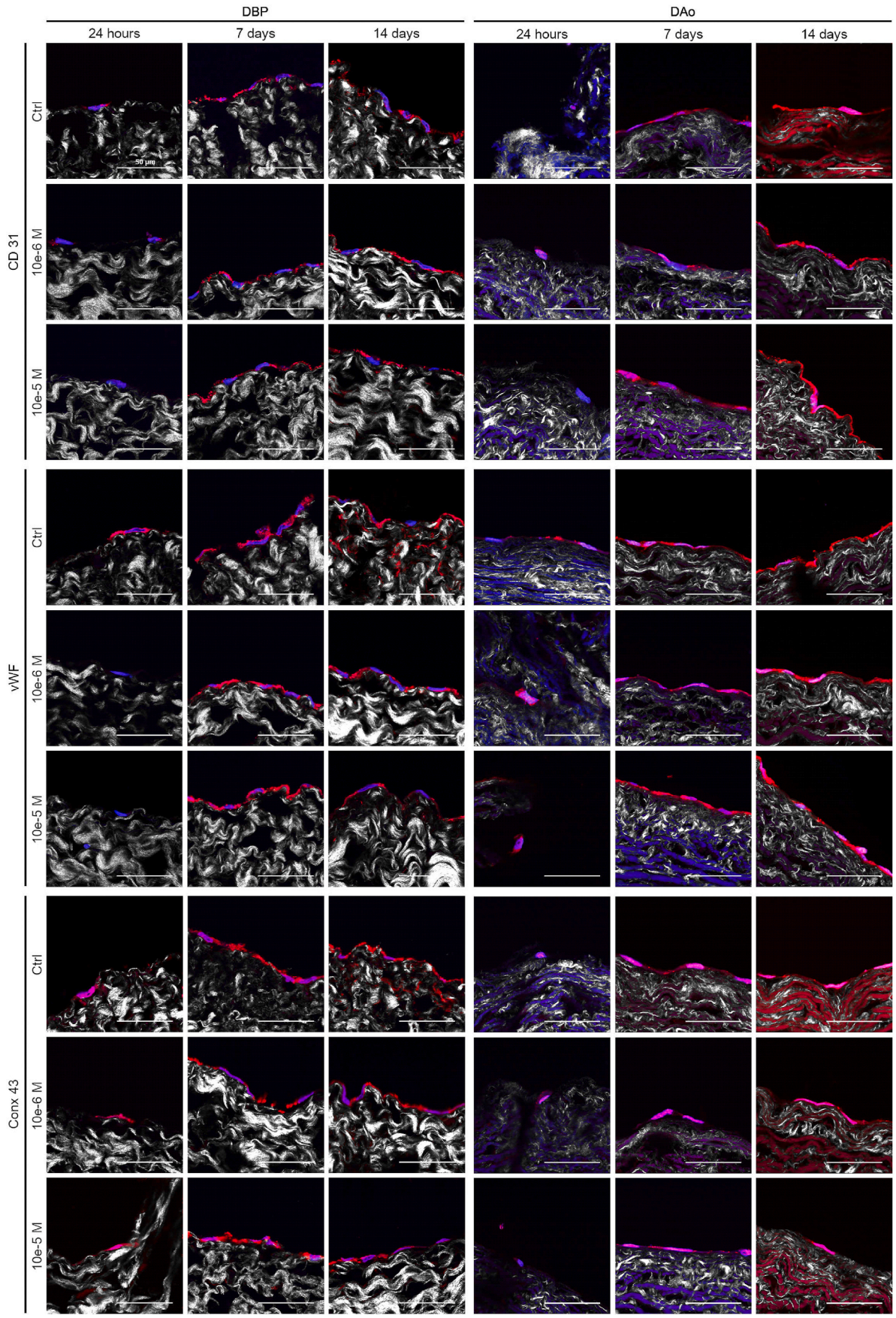

Fig. 7. CD31, vWF and conx43 were expressed in the classical pattern (apart from 24 h) in a continuous-like cell lining in all tissues.

destructive uniaxial loading tests [73], whereas a study was performed on pericardial heterografts to assess the quality control of the mechanical features of glutaraldehyde-fixed leaflets [74]. The site-dependent effects were suitably investigated [73,74].

A pericardial acellular matrix was also developed as a potential candidate especially for heart valve or cardiovascular patching applications [75]. The biochemical and mechanical effects of the cell extraction were assessed [75]. Specifically, fracture tests and viscoelastic analyses generally demonstrated the possibility to preserve the mechanical properties of the fresh tissue in the pericardial acellular matrix [75].

The study of the viscoelastic behavior of pericardial biomaterials clearly requires testing under loading times or frequencies which are typical of those occurring in physiological functions or in a prosthetic device (e.g. heart valve, patching applications) [76]. For this reason, a wide range of experimental mechanical tests was proposed, including stress relaxation, large deformation cyclic loading, and small amplitude forced vibration [76].

As reported in the literature, several methodologies were previously employed to evaluate the mechanical properties of pericardial patches from different mammalian species, the aim being to identify the most suitable biomaterials for the fabrication of high performance and functional prosthetic devices (e.g. heart valves) [77]. Many procedures were described for the evaluation of the mechanical properties (e.g. modulus, strength, strain at break) of pericardial samples, with a special focus on preconditioning (e.g. cyclic loading, pre-stretching) and testing conditions (e.g. uniaxial or biaxial, tensile, flexural, compression, stress-relaxation) [77].

Furthermore, great efforts have been devoted to the optimization of the sterilization methods which may affect the structural and mechanical properties of decellularized tissues. In this context, the efficiency of a two-step sterilization method (i.e. antibiotics/antimycotic cocktail and peracetic acid) was studied for bovine and porcine decellularized pericardium, using an appropriate assessment protocol [78]. The proposed approach was optimized by providing sterile scaffolds for tissue engineering applications. The biocompatibility and structural integrity of the decellularized porcine and bovine tissues were preserved.

Starting from a novel decellularization protocol, decellularized bovine pericardial biological meshes were developed [79]. The structural and mechanical properties were analyzed showing values of elongation and resilience which were higher than those obtained from commercially available devices [79].

However, even though the need for several loading conditions to assess the preservation of the mechanical properties of decellularized tissues has been frequently reported in the literature [71–79], in the current work compression tests were selected to analyze the effect of a covalent functionalization on the mechanical properties (i.e. modulus, maximum stress) of decellularized bovine pericardia and porcine aortas. Briefly, the tests allowed to compare the compressive properties before and after the functionalization process with a REDV tetrapeptide at 10^{-5} M and 10^{-6} M working concentrations.

In particular, compression mechanical tests on DBPs and DAos showed that the functionalization process did not alter the typical high flexibility of the soft biological tissues (i.e. J-shaped stress-strain curve) (Fig. 3c and d) and did not significantly affect the compressive properties (Tables 2 and 3).

Anyway, it is worth noting that in most cases scientific works on decellularized tissues and functionalization processes tend to focus on one or two mechanical characteristics [71,72]. Accordingly, this area should be more thoroughly studied and the present research may be also considered as the first step of a future study in which structural and functional relationships will be deeply analyzed to provide further insight into the determination of the properties of the functionalized tissues.

Although no significant differences were found in terms of compressive mechanical properties between functionalized and untreated samples in the case of DBPs and DAos, the WCA appeared significantly higher for the *serosa* side of functionalized DBPs in comparison with the control group.

The improvement of WCA on REDV-functionalized DBP *serosa* side could result in a protein layer of different composition that could influence EC adhesion. Anyhow Battista et al. [80] have demonstrated that when anchored adhesive motifs are present on or into the biomaterials the cells dig into the physisorbed protein layer and catch the submerged anchored peptides to establish a firmed adhesive structure for finally enhance the stability of cytoskeleton. Therefore, the cellular behavior can nullify the differences among the protein layer composition of surfaces characterized by different WCA. This seems confirmed by biological assays that discriminate between REDV 10^{-5} M and 10^{-6} M functionalization unlike WCA assays. The bioactivity evaluation was performed by static HUVECs seeding. Enhanced adhesion, viability, and proliferation were observed at 24 h and 7 days for the scaffolds functionalized with 10^{-5} M concentration. The study of Aubin et al. [37] demonstrated that the adsorption of REDV on decellularized ovine pericardium enhanced cell viability, but no statistical difference was detected in comparison with the unfunctionalized control. In our study, a clear trend indicating an increased cell adhesion is visible for functionalized tissues, suggesting that the covalent and selective immobilization of this adhesive sequence may be the key to effective endothelialization. The conjugation of a bioactive peptide to a scaffold through a selective functional group, appositely inserted into the peptide sequence, assures an oriented anchorage that is detected and appreciated from cells [81,82]. The article of Battista et al. [80] gives an explanation of the primate of peptide anchoring strategy in comparison with physisorbed peptide one, attributing to the cells the ability to discriminate between bound or physisorbed motifs. At all time-points, the number of dead cells was very limited and non-statistically different among the groups. On day 14, the differences between the functionalized and non-functionalized samples became less pronounced, suggesting that the effect of REDV treatment may be predominant in the early stages of endothelialization. The cytotoxicity was negligible and the proliferation appeared maintained in the REDV groups, confirming the efficacious removal of the reductant, the main concern of the functionalization process for cell viability, but at the same essential to ensure the irreversibility of the covalent bond and a higher yield of peptide grafting reaction on the decellularized ECM (data not shown).

Moreover, for all the groups a positive expression of the classical EC markers CD31 and vWF was demonstrated by immunolabeling, especially from day 7, as a further indication of cell functionality. Histological analyses and conx43 immunolocalization revealed the ongoing development of a continuous-like cell lining that progressively covered the DBP *serosa*. A longer evaluation of seeded scaffolds will be useful to establish whether a complete and stable lining might be achieved and maintained through REDV functionalization.

Finally, even though the small sample size could be considered as a limitation for the current study, the results, however, showed a low variability for each tested group in the different analyses.

5. Conclusions

The REDV selective covalent functionalization of DBP or DAo scaffolds allowed the *in vitro* promotion of earlier endothelial adhesion and proliferation, by a minimal tissue manipulation able to preserve the structure of natural matrices and improve their biological activity. Such a tissue bioengineering strategy could be groundbreaking for any field of surgical therapy involving biological prostheses at the blood interface. High thrombogenic risk is commonly associated with this reconstructive surgery, especially when biological scaffolds or tissues are implanted to replace small diameter vessels and heart valves. Moreover, this biofunctionalization approach could be also applied to develop biological-scaffold-based membranes for a more biocompatible internal lining of blood pumps, as total artificial hearts [83]. With this aim in mind,

further *in vitro* analyses will be performed to thoroughly investigate the effects exerted by REDV-aldehyde functionalization, even at higher concentrations, on the regulatory and migration activities of ECs, also in the settings of anastomotic sites. *In vivo* experiments will be planned to investigate EC lining's stability, viability, and functionality. Furthermore, these analyses will shed light on the biocompatibility of such functionalized ECMs and their ability for *in-situ* accelerated recruitment and adhesion of endogenous ECs in the presence of natural pulsatile blood flow.

Biofunctionalization with REDV or other bioactive peptides could be an effective approach to be used in other reconstruction surgeries where no contact with blood is required, but cell lining is also essential for example in the gastrointestinal and urothelial tracts [84,85].

CRediT authorship contribution statement

Eleonora Dal Sasso: Formal analysis, Writing – original draft, performed the decellularization of the tissues, synthetized REDV peptides and functionalized the scaffolds, performed all the in vitro experiments, performed TP analyses, wrote the paper, all the listed authors contributed to paper proofreading. **Annj Zamuner:** Writing – original draft, synthetized REDV peptides and functionalized the scaffolds, performed WCA and DSC studies, wrote the paper, all the listed authors contributed to paper proofreading. **Andrea Filippi:** Formal analysis, performed TP analyses, all the listed authors contributed to paper proofreading. **Filippo Romanato:** Formal analysis, performed TP analyses, all the listed authors contributed to paper proofreading. **Tiziana Palmosi:** performed the decellularization of the tissues, all the listed authors contributed to paper proofreading. **Luca Vedovelli:** Formal analysis, performed statistical analyses, all the listed authors contributed to paper proofreading. **Dario Gregori:** Formal analysis, performed statistical analyses, all the listed authors contributed to paper proofreading. **José Luís Gómez Ribelles:** Writing – original draft, performed WCA and DSC studies, wrote the paper, all the listed authors contributed to paper proofreading. **Teresa Russo:** performed mechanical compression tests, all the listed authors contributed to paper proofreading. **Antonio Gloria:** Writing – original draft, performed mechanical compression tests, wrote the paper, all the listed authors contributed to paper proofreading. **Laura Iop:** coordinated the study, all the listed authors contributed to paper proofreading. **Gino Gerosa:** Writing – original draft, coordinated the study, all the listed authors contributed to paper proofreading. **Monica Dettin:** coordinated the study, wrote the paper, all the listed authors contributed to paper proofreading.

Declaration of competing interest

The authors declare no competing interests.

Acknowledgments

This work was supported by Padua Heart Program (CA.RI.PA.RO. Foundation) and LIFELAB Program, Consorzio per la Ricerca Sanitaria – CORIS, Veneto Region, Via Giustiniani, 2 – Padova.

JLGR acknowledges financial support from the Spanish State Research Agency (AEI) through the PID2019-106099RB-C41 / AEI / 10.13039/501100011033 project. CIBER-BBN is an initiative funded by the VI National R&D&I Plan 2008–2011, Iniciativa Ingenio 2010, Consolider Program. CIBER Actions are financed by the Instituto de Salud Carlos III with assistance from the European Regional Development Fund.

Appendix A. Supplementary data

Supplementary data related to this article can be found at https://doi.org/10.1016/j.bioactmat.2021.04.003.

References

[1] K.J. Pawlowski, S.E. Rittgers, S.P. Schmidt, G.L. Bowlin, Endothelial cell seeding of polymeric vascular grafts, Front. Biosci. 9 (2004) 1412–1421, https://doi.org/10.2741/1302.

[2] P. Fu, H. Lan, D. Wang, H. Guan, Experimental study on modified treatment and endothelialization of bovine pericardial valves, J. Tongji Med. Univ. 17 (1997) 136–139.

[3] G. Lehner, T. Fischlein, G. Baretton, J.G. Murphy, B. Reichart, Endothelialized biological heart valve prostheses in the non-human primate model, Eur. J. Cardio. Thorac. Surg. 11 (1997) 498–504, https://doi.org/10.1016/S1010-7940(96)01096-2.

[4] K. Jansson, L. Bengtsson, J. Swedenborg, A. Haegerstrand, In vitro endothelialization of bioprosthetic heart valves provides a cell monolayer with proliferative capacities and resistance to pulsatile flow, J. Thorac. Cardiovasc. Surg. 121 (2001) 108–115, https://doi.org/10.1067/mtc.2001.110251.

[5] H. Gulbins, A. Goldemund, I. Anderson, U. Haas, A. Uhlig, B. Meiser, B. Reichart, Preseeding with autologous fibroblasts improves endothelialization of glutaraldehyde-fixed porcine aortic valves, J. Thorac. Cardiovasc. Surg. 125 (2003) 592–601, https://doi.org/10.1067/mtc.2003.48.

[6] J.S. Anderson, T.M. Price, S.R. Hanson, L.A. Harker, In vitro endothelialization of small-caliber vascular grafts, Surgery 101 (1987) 577–586, 0039-6060(87)90300-X.

[7] W. He, Z. Ma, T. Yong, W.E. Teo, S. Ramakrishna, Fabrication of collagen-coated biodegradable polymer nanofiber mesh and its potential for endothelial cells growth, Biomaterials 26 (2005) 7606–7615, https://doi.org/10.1016/j.biomaterials.2005.05.049.

[8] T.W. Chuang, K.S. Masters, Regulation of polyurethane hemocompatibility and endothelialization by tethered hyaluronic acid oligosaccharides, Biomaterials 30 (2009) 5341–5351, https://doi.org/10.1016/j.biomaterials.2009.06.029.

[9] T. Eberl, S. Siedler, B. Schumacher, P. Zilla, K. Schlaudraff, R. Fasol, Experimental in vitro endothelialization of cardiac valve leaflets, Ann. Thorac. Surg. 53 (1992) 487–492, https://doi.org/10.1016/0003-4975(92)90275-9.

[10] T. Fischlein, R. Fasol, In vitro endothelialization of bioprosthetic heart valves, J. Heart Valve Dis. 5 (1996) 58–65.

[11] J.S. Golub, Y. Kim, C.L. Duvall, R.V. Bellamkonda, D. Gupta, A.S. Lin, D. Weiss, W. Robert Taylor, R.E. Guldberg, Sustained VEGF delivery via PLGA nanoparticles promotes vascular growth, Am. J. Physiol. Cell Physiol. 298 (2010) H1959–H1965, https://doi.org/10.1152/ajpheart.00199.2009.

[12] H. Zhang, X. Jia, F. Han, J. Zhao, Y. Zhao, Y. Fan, X. Yuan, Dual-delivery of VEGF and PDGF by double-layered electrospun membranes for blood vessel regeneration, Biomaterials 34 (2013) 2202–2212, https://doi.org/10.1016/j.biomaterials.2012.12.005.

[13] D.H. Walter, M. Cejna, L. Diaz-Sandoval, S. Willis, L. Kirkwood, P.W. Stratford, A. B. Tietz, R. Kirchmair, M. Silver, C. Curry, A. Wecker, Y.S. Yoon, R. Heidenreich, A. Hanley, M. Kearney, F.O. Tio, P. Kuenzler, J.M. Isner, D.W. Losordo, Local gene transfer of phVEGF-2 plasmid by gene-eluting stents: an alternative strategy for inhibition of restenosis, Circulation 110 (2004) 36–45, https://doi.org/10.1161/01.CIR.0000133324.38115.0A.

[14] J. Aoki, P.W. Serruys, H. Van Beusekom, A.T.L. Ong, E.P. McFadden, G. Sianos, W. J. Van Der Giessen, E. Regar, P.J. De Feyter, H.R. Davis, S. Rowland, M.J.B. Kutryk, Endothelial progenitor cell capture by stents coated with antibody against CD34: the HEALING-FIM (healthy endothelial accelerated lining inhibits neointimal growth-first in man) registry, J. Am. Coll. Cardiol. 45 (2005) 1574–1579, https://doi.org/10.1016/j.jacc.2005.01.048.

[15] A.T.L. Ong, J. Aoki, M.J. Kutryk, P.W. Serruys, How to accelerate the endothelialization of stents, Arch. Mal. Coeur. Vaiss. 98 (2005) 123–126.

[16] R. Sethi, C.H. Lee, Endothelial progenitor cell capture stent: safety and effectiveness, J. Intervent. Cardiol. 25 (2012) 493–500, https://doi.org/10.1111/j.1540-8183.2012.00740.x.

[17] W.G. Choi, S.H. Kim, H.S. Yoon, E.J. Lee, D.W. Kim, Impact of an endothelial progenitor cell capturing stent on coronary microvascular function: comparison with drug-eluting stents, Korean J. Intern. Med. 30 (2015) 42, https://doi.org/10.3904/kjim.2015.30.1.42.

[18] D.P. Griese, A. Ehsan, L.G. Melo, D. Kong, L. Zhang, M.J. Mann, R.E. Pratt, R. C. Mulligan, V.J. Dzau, Isolation and transplantation of autologous circulating endothelial cells into denuded vessels and prosthetic grafts: implications for cell-based vascular therapy, Circulation 108 (2003) 2710–2715, https://doi.org/10.1161/01.CIR.0000096490.16596.A6.

[19] B.D. Markway, O.J.T. McCarty, U.M. Marzec, D.W. Courtman, S.R. Hanson, M. T. Hinds, Capture of flowing endothelial cells using surface-immobilized anti-kinase insert domain receptor antibody, Tissue Eng. C Methods 14 (2008) 97–105, https://doi.org/10.1089/ten.tec.2007.0300.

[20] J.E. Jordan, J.K. Williams, S.J. Lee, D. Raghavan, A. Atala, J.J. Yoo, Bioengineered self-seeding heart valves, J. Thorac. Cardiovasc. Surg. 143 (2012) 201–208, https://doi.org/10.1016/j.jtcvs.2011.10.005.

[21] J.K. Williams, E.S. Miller, M.R. Lane, A. Atala, J.J. Yoo, J.E. Jordan, Characterization of CD133 antibody-directed recellularized heart valves, J. Cardiovasc. Transl. Res. 8 (2015) 411–420, https://doi.org/10.1007/s12265-015-9651-3.

[22] U. Hersel, C. Dahmen, H. Kessler, RGD modified polymers: biomaterials for stimulated cell adhesion and beyond, Biomaterials 24 (2003) 4385–4415, https://doi.org/10.1016/S0142-9612(03)00343-0.

[23] H.B. Lin, C. García-Echeverría, S. Asakura, W. Sun, D.F. Mosher, S.L. Cooper, Endothelial cell adhesion on polyurethanes containing covalently attached RGD-

peptides, Biomaterials 13 (1992) 905–914, https://doi.org/10.1016/0142-9612(92)90113-3.
[24] J. Zhou, B. Nie, Z. Zhu, J. Ding, W. Yang, J. Shi, X. Dong, J. Xu, N. Dong, Promoting endothelialization on decellularized porcine aortic valve by immobilizing branched polyethylene glycolmodified with cyclic-RGD peptide: an in vitro study, Biomed. Mater. 10 (2015), 065014, https://doi.org/10.1088/1748-6041/10/6/065014.
[25] R. Pytela, M. Pierschbacher, M. Ginsberg, E. Plow, E. Ruoslahti, Platelet membrane glycoprotein IIb/IIIa: member of a family of Arg-Gly-Asp–specific adhesion receptors, Science (80-.) 231 (1986) 1559–1562, https://doi.org/10.1126/science.2420006.
[26] D.R. Phillips, I.F. Charo, L. V Parise, L.A. Fitzgerald, The platelet membrane glycoprotein IIb-IIIa complex, Blood 71 (1988) 831–843.
[27] M.J. Humphries, S.K. Akiyama, A. Komoriya, K. Olden, K.M. Yamada, Identification of an alternatively spliced site in human plasma fibronectin that mediates cell type-specific adhesion, J. Cell Biol. 103 (1986) 2637–2647, https://doi.org/10.1083/jcb.103.6.2637.
[28] A.P. Mould, A. Komoriya, K.M. Yamada, M.J. Humphries, The CS5 peptide is a second site in the IIICS region of fibronectin recognized by the integrin α4β1: inhibition of α4β1function by RGD peptide homologues, J. Biol. Chem. 266 (1991) 3579–3585.
[29] J.A. Hubbell, S.P. Massia, N.P. Desai, P.D. Drumheller, Endothelial cell-selective materials for tissue engineering in the vascular graft via a new receptor, Nat. Biotechnol. 9 (1991) 568–572, https://doi.org/10.1038/nbt0691-568.
[30] S.P. Massia, J.A. Hubbell, Vascular endothelial cell adhesion and spreading promoted by the peptide REDV of the IIICS region of plasma fibronectin is mediated by integrin alpha4beta1, J. Biol. Chem. 267 (1992) 14019–14026.
[31] X. Ren, Y. Feng, J. Guo, H. Wang, Q. Li, J. Yang, X. Hao, J. Lv, N. Ma, W. Li, Surface modification and endothelialization of biomaterials as potential scaffolds for vascular tissue engineering applications, Chem. Soc. Rev. 44 (2015) 5680–5742, https://doi.org/10.1039/c4cs00483c.
[32] B. Butruk, P. Bąbik, B. Marczak, T. Ciach, Surface endothelialization of polyurethanes, Procedia Eng 59 (2013) 126–132, https://doi.org/10.1016/j.proeng.2013.05.101.
[33] J. Yang, M. Khan, L. Zhang, X. Ren, J. Guo, Y. Feng, S. Wei, W. Zhang, Antimicrobial surfaces grafted random copolymers with REDV peptide beneficial for endothelialization, J. Mater. Chem. B. 3 (2015) 7682–7697, https://doi.org/10.1039/c5tb01155h.
[34] B.A. Butruk-Raszeja, M.S. Dresler, A. Kuźmińska, T. Ciach, Endothelialization of polyurethanes: surface silanization and immobilization of REDV peptide, Colloids Surf. B Biointerfaces 144 (2016) 335–343, https://doi.org/10.1016/j.colsurfb.2016.04.017.
[35] S. Yu, Y. Gao, X. Mei, T. Ren, S. Liang, Z. Mao, C. Gao, Preparation of an Arg-Glu-Asp-Val peptide density gradient on hyaluronic acid-coated poly(μ-caprolactone) film and its influence on the selective adhesion and directional migration of endothelial cells, ACS Appl. Mater. Interfaces 8 (2016) 29280–29288, https://doi.org/10.1021/acsami.6b09375.
[36] S.C. Heilshorn, K.A. DiZio, E.R. Welsh, D.A. Tirrell, Endothelial cell adhesion to the fibronectin CS5 domain in artificial extracellular matrix proteins, Biomaterials 24 (2003) 4245–4252, https://doi.org/10.1016/S0142-9612(03)00294-1.
[37] H. Aubin, C. Mas-Moruno, M. Iijima, N. Schütterle, M. Steinbrink, A. Assmann, F. J. Gil, A. Lichtenberg, M. Pegueroles, P. Akhyari, Customized interface biofunctionalization of decellularized extracellular matrix: toward enhanced endothelialization, Tissue Eng. C Methods (2016), https://doi.org/10.1089/ten.tec.2015.0556.
[38] M. Spina, F. Ortolani, A. El Messlemani, A. Gandaglia, J. Bujan, N. Garcia-Honduvilla, I. Vesely, G. Gerosa, D. Casarotto, L. Petrelli, M. Marchini, Isolation of intact aortic valve scaffolds for heart-valve bioprostheses: extracellular matrix structure, prevention from calcification, and cell repopulation features, J. Biomed. Mater. Res. 67 (2003) 1338–1350, https://doi.org/10.1002/jbm.a.20025.
[39] L. Iop, A. Bonetti, F. Naso, S. Rizzo, S. Cagnin, R. Bianco, C. Dal Lin, P. Martini, H. Poser, P. Franci, G. Lanfranchi, R. Busetto, M. Spina, C. Basso, M. Marchini, A. Gandaglia, F. Ortolani, G. Gerosa, Decellularized allogeneic heart valves demonstrate self-regeneration potential after a long-term preclinical evaluation, PloS One 9 (2014), e99593, https://doi.org/10.1371/journal.pone.0099593.
[40] S. Zouhair, E. Dal Sasso, S.R. Tuladhar, C. Fidalgo, L. Vedovelli, A. Filippi, G. Borile, A. Bagno, M. Marchesan, D.R. Giorgio, D. Gregori, W.F. Wolkers, F. Romanato, S. Korossis, G. Gerosa, L. Iop, A comprehensive comparison of bovine and porcine decellularized pericardia: new insights for surgical applications, Biomolecules 10 (2020) 371, https://doi.org/10.3390/biom10030371.
[41] A. Filippi, E. Dal Sasso, L. Iop, A. Armani, M. Gintoli, M. Sandri, G. Gerosa, F. Romanato, G. Borile, Multimodal label-free ex vivo imaging using a dual-wavelength microscope with axial chromatic aberration compensation, J. Biomed. Opt. 23 (2018) 1, https://doi.org/10.1117/1.JBO.23.9.091403.
[42] S. Zouhair, P. Aguiari, L. Iop, A. Vásquez-Rivera, A. Filippi, F. Romanato, S. Korossis, W.F. Wolkers, G. Gerosa, Preservation strategies for decellularized pericardial scaffolds for off-the-shelf availability, Acta Biomater. (2018), https://doi.org/10.1016/j.actbio.2018.10.026.
[43] G.A. Grant, Synthetic Peptides : a User's Guide, Oxford University Press, 2002.
[44] A. Schwartz, L. Wang, E. Early, A. Gaigalas, Y.Z. Zhang, G.E. Marti, R.F. Vogt, Quantitating fluorescence intensity from fluorophore: the definition of MESF assignment, J. Res. Natl. Inst. Stand. Technol. 107 (2002) 83, https://doi.org/10.6028/jres.107.009.
[45] A.K. Gaigalas, L.L. Wang, A. Schwartz, G.E. Marti, R.F. Vogt, Quantitating fluorescence intensity from fluorophore: assignment of MESF values, J. Res. Natl. Inst. Stand. Technol. 110 (2005) 101, https://doi.org/10.6028/jres.110.010.
[46] J. Schindelin, I. Arganda-Carreras, E. Frise, V. Kaynig, M. Longair, T. Pietzsch, S. Preibisch, C. Rueden, S. Saalfeld, B. Schmid, J.Y. Tinevez, D.J. White, V. Hartenstein, K. Eliceiri, P. Tomancak, A. Cardona, Fiji: an open-source platform for biological-image analysis, Nat. Methods 9 (2012) 676–682, https://doi.org/10.1038/nmeth.2019.
[47] International Organization for Standardization, ISO 10993-5 Biological Evaluation of Medical Devices - Part 5: Tests for in Vitro Cytotoxicity, 2009, p. 34.
[48] M. Granados, L. Morticelli, S. Andriopoulou, P. Kalozoumis, M. Pflaum, P. Iablonskii, B. Glasmacher, M. Harder, J. Hegermann, C. Wrede, I. Tudorache, S. Cebotari, A. Hilfiker, A. Haverich, S. Korossis, Development and characterization of a porcine mitral valve scaffold for tissue engineering, J. Cardiovasc. Transl. Res. 10 (2017) 374–390, https://doi.org/10.1007/s12265-017-9747-z.
[49] S. Cebotari, I. Tudorache, T. Jaekel, A. Hilfiker, S. Dorfman, W. Ternes, A. Haverich, A. Lichtenberg, Detergent decellularization of heart valves for tissue engineering: toxicological effects of residual detergents on human endothelial cells, Artif. Organs 34 (2010) 206–210, https://doi.org/10.1111/j.1525-1594.2009.00796.x.
[50] X. Wang, B. Ding, J. Yu, M. Wang, Engineering biomimetic superhydrophobic surfaces of electrospun nanomaterials, Nano Today (2011), https://doi.org/10.1016/j.nantod.2011.08.004.
[51] H.C. Chen, C.H. Tsai, M.C. Yang, Mechanical properties and biocompatibility of electrospun polylactide/poly(vinylidene fluoride) mats, J. Polym. Res. (2011), https://doi.org/10.1007/s10965-010-9421-5.
[52] A.C. Areias, C. Ribeiro, V. Sencadas, N. Garcia-Giralt, A. Diez-Perez, J.L. Gómez Ribelles, S. Lanceros-Méndez, Influence of crystallinity and fiber orientation on hydrophobicity and biological response of poly(l-lactide) electrospun mats, Soft Matter (2012), https://doi.org/10.1039/c2sm25557j.
[53] M. Ma, Y. Mao, M. Gupta, K.K. Gleason, G.C. Rutledge, Superhydrophobic fabrics produced by electrospinning and chemical vapor deposition, Macromolecules (2005), https://doi.org/10.1021/ma0511189.
[54] W.F. Harrington, P.H. Von Hippel, The structure of collagen and gelatin, Adv. Protein Chem. 16 (1962) 1–138, https://doi.org/10.1016/S0065-3233(08)60028-5.
[55] P.L. Privalov, E.I. Tiktopulo, V.M. Tischenko, Stability and mobility of the collagen structure, J. Mol. Biol. 127 (1979) 203–216, https://doi.org/10.1016/0022-2836(79)90240-7.
[56] V. Samouillan, F. Delaunay, J. Dandurand, N. Merbahi, J.-P. Gardou, M. Yousfi, A. Gandaglia, M. Spina, C. Lacabanne, The use of thermal techniques for the characterization and selection of natural biomaterials, J. Funct. Biomater. 2 (2011) 230–248, https://doi.org/10.3390/jfb2030230.
[57] B.D. Ratner, Blood compatibility–a perspective, J. Biomater. Sci. Polym. Ed. 11 (2000) 1107–1119.
[58] B.D. Ratner, The blood compatibility catastrophe, J. Biomed. Mater. Res. 27 (1993) 283–287, https://doi.org/10.1002/jbm.820270302.
[59] B.D. Ratner, The catastrophe revisited: blood compatibility in the 21st Century, Biomaterials 28 (2007) 5144–5147, https://doi.org/10.1016/j.biomaterials.2007.07.035.
[60] I. Sotiri, M. Robichaud, D. Lee, S. Braune, M. Gorbet, B.D. Ratner, J.L. Brash, R. A. Latour, I. Reviakine, BloodSurf 2017: news from the blood-biomaterial frontier, Acta Biomater. 87 (2019) 55–60, https://doi.org/10.1016/j.actbio.2019.01.032.
[61] M. Weber, H. Steinle, S. Golombek, L. Hann, C. Schlensak, H.P. Wendel, M. Avci-Adali, Blood-contacting biomaterials: in vitro evaluation of the hemocompatibility, Front. Bioeng. Biotechnol. (2018), https://doi.org/10.3389/fbioe.2018.00099.
[62] J. Ward, J. Kelly, W. Wang, D.I. Zeugolis, A. Pandit, Amine functionalization of collagen matrices with multifunctional polyethylene glycol systems, Biomacromolecules 11 (2010) 3093–3101, https://doi.org/10.1021/bm100898p.
[63] X. Dong, X. Wei, W. Yi, C. Gu, X. Kang, Y. Liu, Q. Li, D. Yi, RGD-modified acellular bovine pericardium as a bioprosthetic scaffold for tissue engineering, J. Mater. Sci. Mater. Med. 20 (2009) 2327–2336, https://doi.org/10.1007/s10856-009-3791-4.
[64] J. Devalliere, Y. Chen, K. Dooley, M.L. Yarmush, B.E. Uygun, Improving functional re-endothelialization of acellular liver scaffold using REDV cell-binding domain, Acta Biomater. 78 (2018) 151–164, https://doi.org/10.1016/j.actbio.2018.07.046.
[65] M. Yamauchi, M. Sricholpech, Lysine post-translational modifications of collagen, Essays Biochem. 52 (2012) 113–133, https://doi.org/10.1042/bse0520113.
[66] H.W. Jun, J.L. West, Modification of polyurethaneurea with PEG and YIGSR peptide to enhance endothelialization without platelet adhesion, J. Biomed. Mater. Res. B Appl. Biomater. 72 (2005) 131–139, https://doi.org/10.1002/jbm.b.30135.
[67] H. Wang, Y. Feng, J. Yang, J. Guo, W. Zhang, Targeting REDV peptide functionalized polycationic gene carrier for enhancing the transfection and migration capability of human endothelial cells, J. Mater. Chem. B. 3 (2015) 3379–3391, https://doi.org/10.1039/c4tb02019g.
[68] M.I. Castellanos, A.S. Zenses, A. Grau, J.C. Rodríguez-Cabello, F.J. Gil, J. M. Manero, M. Pegueroles, Biofunctionalization of REDV elastin-like recombinamers improves endothelialization on CoCr alloy surfaces for cardiovascular applications, Colloids Surf. B Biointerfaces 127 (2015) 22–32, https://doi.org/10.1016/j.colsurfb.2014.12.056.
[69] J. Zhou, J. Ding, B. Nie, S. Hu, Z. Zhu, J. Chen, J. Xu, J. Shi, N. Dong, Promotion of adhesion and proliferation of endothelial progenitor cells on decellularized valves by covalent incorporation of RGD peptide and VEGF, J. Mater. Sci. Mater. Med. 27 (2016) 142, https://doi.org/10.1007/s10856-016-5750-1.
[70] Y. Ji, Y. Wei, X. Liu, J. Wang, K. Ren, J. Ji, Zwitterionic polycarboxybetaine coating functionalized with REDV peptide to improve selectivity for endothelial cells, J. Biomed. Mater. Res. 100 A (2012) 1387–1397, https://doi.org/10.1002/jbm.a.34077.

[71] F. Wang, J. Guan Jianjun, Cellular cardiomyoplasty and cardiac tissue engineering for myocardial therapy, Adv. Drug Deliv. Rev. (2010), https://doi.org/10.1016/j.addr.2010.03.001.
[72] E. García-Gareta, Y. Abduldaiem, P. Sawadkar, C. Kyriakidis, F. Lali, K.V. Greco, Decellularised scaffolds: just a framework? Current knowledge and future directions, J. Tissue Eng. (2020), https://doi.org/10.1177/2041731420942903.
[73] C.E. Crofts, E.A. Trowbridge, The tensile strength of natural and chemically modified bovine pericardium, J. Biomed. Mater. Res. (1988), https://doi.org/10.1002/jbm.820220202.
[74] E.A. Trowbridge, K.M. Roberts, C.E. Crofts, P.V. Lawford, Pericardial heterografts, Toward quality control of the mechanical properties of glutaraldehyde-fixed leaflets, J. Thorac. Cardiovasc. Surg. (1986), https://doi.org/10.1016/s0022-5223(19)35927-6.
[75] D.W. Courtman, C.A. Pereira, V. Kashef, D. McComb, J.M. Lee, G.J. Wilson, Development of a pericardial acellular matrix biomaterial: biochemical and mechanical effects of cell extraction, J. Biomed. Mater. Res. 28 (1994) 655–666, https://doi.org/10.1002/jbm.820280602.
[76] J.M. Lee, S.A. Haberer, C.A. Pereira, W.A. Naimark, D.W. Courtman, G.J. Wilson, High strain rate testing and structural analysis of pericardial bioprosthetic materials, in: ASTM Spec. Tech. Publ., 1994, https://doi.org/10.1520/stp18091s.
[77] P. Aguiari, M. Fiorese, L. Iop, G. Gerosa, A. Bagno, Mechanical testing of pericardium for manufacturing prosthetic heart valves, Interact. Cardiovasc. Thorac. Surg. 22 (2016) 72–84, https://doi.org/10.1093/icvts/ivv282.
[78] C. Fidalgo, L. Iop, M. Sciro, M. Harder, D. Mavrilas, S. Korossis, A. Bagno, G. Palù, P. Aguiari, G. Gerosa, A sterilization method for decellularized xenogeneic cardiovascular scaffolds, Acta Biomater. 67 (2018) 282–294, https://doi.org/10.1016/j.actbio.2017.11.035.
[79] A. Bielli, R. Bernardini, D. Varvaras, P. Rossi, G. Di Blasi, G. Petrella, O. C. Buonomo, M. Mattei, A. Orlandi, Characterization of a new decellularized bovine pericardial biological mesh: structural and mechanical properties, J. Mech. Behav. Biomed. Mater. (2018), https://doi.org/10.1016/j.jmbbm.2017.12.003.
[80] E. Battista, F. Causa, V. Lettera, V. Panzetta, D. Guarnieri, S. Fusco, F. Gentile, P. A. Netti, Ligand engagement on material surfaces is discriminated by cell mechanosensoring, Biomaterials (2015), https://doi.org/10.1016/j.biomaterials.2014.12.012.
[81] M. Dettin, T. Herath, R. Gambaretto, G. Iucci, C. Battocchio, A. Bagno, F. Ghezzo, C. Di Bello, G. Polzonetti, L. Di Silvio, Assessment of novel chemical strategies for covalent attachment of adhesive peptides to rough titanium surfaces: XPS analysis and biological evaluation, J. Biomed. Mater. Res. (2009), https://doi.org/10.1002/jbm.a.32222.
[82] P. Brun, M. Scorzeto, S. Vassanelli, I. Castagliuolo, G. Palù, F. Ghezzo, G.M. L. Messina, G. Iucci, V. Battaglia, S. Sivolella, A. Bagno, G. Polzonetti, G. Marletta, M. Dettin, Mechanisms underlying the attachment and spreading of human osteoblasts: from transient interactions to focal adhesions on vitronectin-grafted bioactive surfaces, Acta Biomater. (2013), https://doi.org/10.1016/j.actbio.2012.12.018.
[83] E. Dal Sasso, A. Bagno, S.T.G. Scuri, G. Gerosa, L. Iop, The biocompatibility challenges in the total artificial heart evolution, Annu. Rev. Biomed. Eng. 21 (2019) 85–110, https://doi.org/10.1146/annurev-bioeng-060418-052432.
[84] D.F. Williams, Challenges with the development of biomaterials for sustainable tissue engineering, Front. Bioeng. Biotechnol. 7 (2019), https://doi.org/10.3389/fbioe.2019.00127.
[85] Q. Wan, G. Xiong, G. Liu, T.D. Shupe, G. Wei, D. Zhang, D. Liang, X. Lu, A. Atala, Y. Zhang, Urothelium with barrier function differentiated from human urine-derived stem cells for potential use in urinary tract reconstruction, Stem Cell Res. Ther. 9 (2018) 304, https://doi.org/10.1186/s13287-018-1035-6.